The 2009 IEEE/RSJ International Conference on
Intelligent Robots and Systems
October 11-15, 2009 St. Louis, USA

Fiber-reinforced Conjugated Polymer Torsional Actuator and Its Nonlinear Elasticity Modeling

Yang Fang, Thomas J. Pence and Xiaobo Tan

Abstract— **Reported conjugated polymer actuators have typically been limited to bender or linear extender configurations. In this paper, we present a fiber-reinforced conjugated polymer actuator capable of torsional motion. By incorporating platinum fibers into the material matrix during the electrochemical fabrication process, we create anisotropy in the interaction between the fiber and the material matrix, resulting in torsion and other associated deformations upon actuation. A nonlinear elasticity-based model is utilized to capture the actuator performance for both small and large deformations. The effectiveness of the model is verified through comparison with experimental results.**

I. INTRODUCTION

Conjugated polymers, such as polypyrrole (PPy), are one class of electroactive polymers that have inherent actuation and sensing properties, with promising applications in robotics and micro systems [1]–[3]. Upon application of a potential (or voltage), a conjugated polymer in contact with a proper electrolyte undergoes reduction/oxidation (redox), where ions from the electrolyte move in and out of the polymer matrix. The volume change induced by such ion transport is considered to be the primary mechanism of actuation for conjugated polymers [2]. The strains generated by PPy actuators are typically between 1% and 10% [1]. Conjugated polymer actuators have numerous potential applications in microfluidic and medical devices [4]–[7].

Reported conjugate polymer actuators have typically been limited to bender [2], [8] or linear extender [1] configurations. However, in microsurgery and other robotic applications, more complicated actuator motions will be required. It is known that fiber-reinforced elastic material can generate complicated deformation [9]–[11]. The anisotropy associated with the interaction between the fibers and the material matrix makes the material resist elongation in certain directions, which generates torsional motion when the volume of the material changes [12]. This principle provides a potentially useful approach to fabricating compact torsional actuators using conjugated polymers. These polymers provide an ideal material to realize the design of fiber-reinforced elastic material actuators in practice, since the volume of the polymer can be changed easily with electrical actuation.

A conjugated polymer tube was fabricated by Ding *et al*. [13], where platinum wires were integrated into the conjugated polymer during the fabrication process. However, the purpose for the platinum wires in that paper was to increase the electrical conductivity along the tube, so the torsional motion introduced by the fiber-reinforced structure was not investigated. To the best of the authors' knowledge, there has been no detailed investigation on torsional motion in fiber-reinforced conjugated polymer actuators.

In this paper, torsional motion of a fiber-reinforced conjugated polymer actuator is investigated. A nonlinear elasticity-based model is proposed to capture voltage-induced torsion and other associated deformations of the conjugated polymer tube. The model is verified with experimental measurements made on a platinum fiber-reinforced PPy tube.

The remainder of the paper is organized as follows. The actuation mechanism and actuator configuration are introduced in Section II. The nonlinear elasticity model is presented in Section III. Actuator fabrication and model validation are discussed in Section IV. Finally the conclusions are provided in Section V.

II. ACTUATOR MECHANISM

Fig. 1 illustrates the mechanism of a PPy actuator in electrolyte. If a voltage is applied across the PPy actuator and the electrolyte, the ions in the electrolyte will move towards and accumulate at the interface between the PPy and the electrolyte. The highly concentrated ions in the double layer will diffuse into the PPy layer, and oxidize the PPy polymer. When a negative voltage is applied, the PPy polymer is reduced, in the sense that the ions will be repelled out of the PPy polymer chain and move back to the electrolyte. Because of the mass transfer introduced by this ion movement, the volume of PPy will expand (oxidation) or shrink (reduction). This concept has been utilized to generate bending and linear motion [1]–[3].

The oxidation dynamics mainly involves diffusion and migration effects [14]. When a DC voltage U is applied across the polymer, quasi-static analysis can be applied [15]. The total transferred charges can be calculated as

$$Q = k_1 \cdot U, \tag{1}$$

where $k_1 = \frac{1}{2}(1+\frac{h}{\delta})C$, h is the thickness of the PPy layer, δ is the thickness of the double-layer at the polymer/electrolyte interface, and C is the double-layer capacitance. The proportionality constant k_1 can be obtained based on experiments.

The work of Y. Fang and X. Tan was supported in part by an NSF CAREER grant (ECCS 0547131) and MSU IRGP (05-IRGP-418), and the work of T. Pence was supported by an NSF grant (CMMI 0510600).

Yang Fang and Xiaobo Tan are with the Smart Microsystems Laboratory, Department of Electrical & Computer Engineering, Michigan State University, East Lansing, MI 48824 USA fangyang@msu.edu (Y.F.), xbtan@egr.msu.edu (X.T.)

Thomas J. Pence is with the Department of Mechanical Engineering, Michigan State University, East Lansing, MI 48824 USA pence@egr.msu.edu

Send correspondence to X. Tan. Tel: 517-432-5671; Fax: 517-353-1980

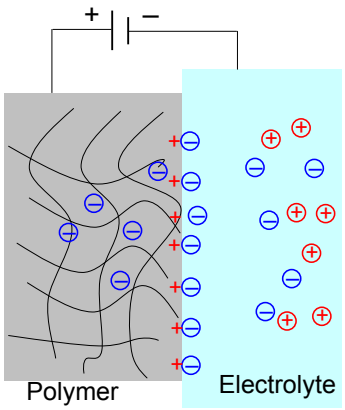

Fig. 1. Illustration of double-layer charging and diffusion for a conjugated polymer film with one side in contact with electrolyte.

From (1), the transferred charge density ρ can be obtained as

$$\rho = \frac{Q}{V}, \tag{2}$$

where V is the volume of the PPy layer. Those ions transferred to the PPy polymer result in volume change, which can be captured by [16]:

$$\nu = \frac{V - k_2 \rho V}{V} = 1 - k_2 \rho, \tag{3}$$

where ν represents the swelling ratio of the PPy layer, and k_2 is the swelling-to-charge ratio. When $\nu > 1$, the volume is increased; when $\nu < 1$, the volume is decreased. The value of k_2 has the order of $10^{-10}\mathrm{m}^3 \cdot \mathrm{C}^{-1}$ [17].

Fiber-reinforced elastic materials can generate complicated deformation when subject to swelling. When the fibers are aligned in special ways, the material matrix containing fibers will expand in the direction perpendicular to the fiber [12]. A specific case is studied in this paper, where the fiber is helically wound about a elastic tube with a fixed pitch angle, which is illustrated in Fig. 2. The elastic material we consider here is PPy, the volume of which can be changed through electrical activation. Theoretical analysis shows that the tube will generate torsional motion when subject to swelling. Platinum wires are chosen to be integrated into PPy tube during the fabrication with some pitch angle β.

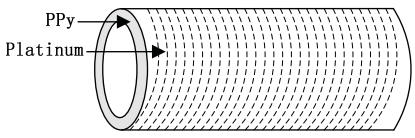

Fig. 2. Schematic of the conjugated polymer-based torsional actuator.

III. Nonlinear Mechanical Model Based on a Swelling Framework

A. Nonlinear Mechanical Modeling Framework

The original and deformed configurations are shown in Fig. 3, where $\mathbf{F}$ represents the deformation gradient, which can map vectors (expressed in $\mathrm{Z}, \mathrm{R}, \Theta$ domain) in the original configuration to vectors (expressed in z, r, θ domain) in the deformed configuration. The pitch angle is defined as β ($0 < \beta < 90^o$) [12].

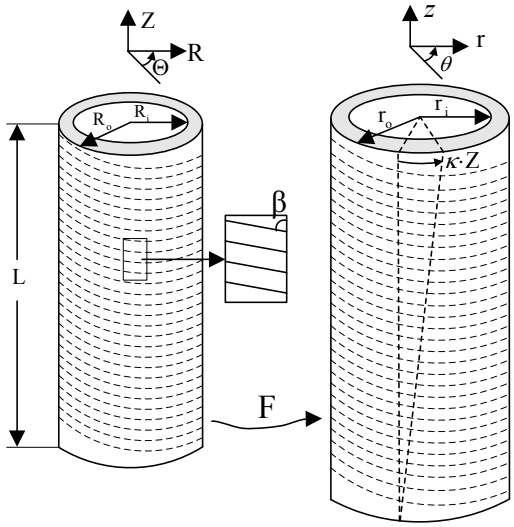

Fig. 3. Illustration of the actuator configuration. Left: original configuration; right: deformed configuration.

The deformation can be characterized by the following equation:

$$r = r(R), \quad \theta = \Theta + \kappa \mathrm{Z}, \quad z = \lambda_z \mathrm{Z}, \tag{4}$$

where κ is the twist per unit length, and λ_z is the elongation per unit length in the longitudinal direction. Suppose that the deformation takes a particle at location $\mathbf{X}$ in the reference configuration to the location $\mathbf{x}$ in the deformed configuration. The deformation gradient is defined as

$$\mathbf{F} = \frac{\partial \mathbf{x}}{\partial \mathbf{X}}, \tag{5}$$

where

$$\begin{aligned} d\mathbf{X} &= dR\,\mathbf{e}_R + R d\Theta\,\mathbf{e}_\Theta + dZ\,\mathbf{e}_Z, \\ d\mathbf{x} &= dr\,\mathbf{e}_r + r d\theta\,\mathbf{e}_\theta + dz\,\mathbf{e}_z, \end{aligned}$$

$\mathbf{e}_R, \mathbf{e}_\Theta$, and $\mathbf{e}_Z$ are the orthonormal unit vectors in the original configuration, and $\mathbf{e}_r, \mathbf{e}_\theta$,and $\mathbf{e}_z$ are the orthonormal unit vectors in the deformed configuration. The deformation gradient tensor is

$$\mathbf{F} = \frac{dr}{dR}\mathbf{e}_r \otimes \mathbf{e}_R + \frac{r}{R}\mathbf{e}_\theta \otimes \mathbf{e}_\Theta + \kappa r \mathbf{e}_\theta \otimes \mathbf{e}_Z + \lambda_z \mathbf{e}_z \otimes \mathbf{e}_Z, \tag{6}$$

where $\otimes$ is the dyadic product. We assume that PPy is mechanically incompressible both before and after swelling. This assumption is based on relevant literature [18]. So the deformation satisfies the constraint that the volume is not changed by the deformation after swelling, which means

$$\det \mathbf{F} = \nu. \tag{7}$$

This, together with (6), implies

$$\frac{1}{R}\lambda_z r\frac{dr}{dR}=\nu. \tag{8}$$

Rewriting (8) as $rdr=\frac{\nu}{\lambda_z}RdR$ and integrating, we get

$$r^2=r_i^2+\frac{2}{\lambda_z}\int_{R_i}^{R}\nu RdR, \tag{9}$$

where r_i and R_i are the inner radii of the tube in the original configuration and the deformed configuration, respectively. The left Cauchy-Green deformation tensor is defined by

$$\mathbf{B}=\mathbf{F}\mathbf{F}^{\mathbf{T}}. \tag{10}$$

Following (6) and (8), we can further express $\mathbf{B}$ as

$$\begin{aligned}\mathbf{B} &= \frac{\nu^2R^2}{\lambda_z^2r^2}\mathbf{e}_r\otimes\mathbf{e}_r+(\kappa^2+\frac{1}{R^2})r^2\mathbf{e}_\theta\otimes\mathbf{e}_\Theta\\ &\quad+\kappa\lambda_z r(\mathbf{e}_\theta\otimes\mathbf{e}_z+\mathbf{e}_z\otimes\mathbf{e}_\theta)+\lambda_z^2\mathbf{e}_z\otimes\mathbf{e}_z.\end{aligned} \tag{11}$$

The principal invariants of $\mathbf{B}$ are defined as

$$I_1=\mathrm{tr}(\mathbf{B}),\ \ I_2=I_3\mathrm{tr}(\mathbf{B}^{-1}),\ \ I_3=\det(\mathbf{B}). \tag{12}$$

From (6), the invariant I_1 is obtained as

$$I_1=\frac{\nu^2R^2}{\lambda_z^2r^2}+\frac{r^2}{R^2}+\kappa^2r^2+\lambda_z^2. \tag{13}$$

The elastic energy function of PPy can be denoted by Φ_m and modeled in the neo-Hookean form as

$$\Phi_m=\frac{1}{2}\mu(I_1-3\nu^{2/3}), \tag{14}$$

where μ is a material elastic constant that can be taken as $E_{PPy}/3$, and E_{PPy} is the Young's modulus [15].

Let $\mathbf{M}$ be the unit vector in the reference configuration that defines the fiber direction in the material matrix:

$$\mathbf{M}=\sin\beta\mathbf{e}_\Theta+\cos\beta\mathbf{e}_Z, \tag{15}$$

where β is the pitch angle defined in Fig. 3. Given the deformation gradient $\mathbf{F}$, the unit vector $\mathbf{M}$ is mapped into

$$\mathbf{m}=\mathbf{F}\mathbf{M}=(\kappa\cos\beta+\frac{1}{R}\sin\beta)\gamma\mathbf{e}_\theta+\lambda_z\cos\beta\mathbf{e}_z. \tag{16}$$

The square of the stretch of the fiber under actuation is

$$I_4=\mathrm{tr}(\mathbf{m}\otimes\mathbf{m})=(\kappa\cos\beta+\frac{1}{R}\sin\beta)^2\gamma^2+\lambda_z^2\cos^2\beta. \tag{17}$$

The strain energy function of the fiber can be modeled as

$$\Phi_f=\frac{1}{2}\gamma(I_4-1)^2, \tag{18}$$

where γ is another material constant. This material constant will depend on the volume fraction of fibers in the overall composite. Using the connection between the nonlinear theory and the linear theory of anisotropic elasticity [19], we may take $\gamma=\frac{1}{5}E_{platinum}$ in this investigation. Therefore, the total energy of the fiber-reinforced PPy actuator is

$$W=\Phi_m+\Phi_f. \tag{19}$$

The Cauchy stress tensor is [12]

$$\sigma=\frac{1}{\nu}\frac{\partial W}{\partial\mathbf{F}}\mathbf{F}^T-p\mathbf{I}, \tag{20}$$

where p has the interpretation of the (unknown) hydrostatic pressure. With the expression of total energy in (19), the Cauchy stress can be written as [12]

$$\sigma=\frac{2}{\nu}\frac{\partial\Phi_m}{\partial I_1}\mathbf{B}+\frac{2}{\nu}\frac{\partial\Phi_f}{\partial I_4}\mathbf{m}\otimes\mathbf{m}-p\mathbf{I}. \tag{21}$$

Considering (11) and (16), we can express (21) as

$$\begin{aligned}\sigma &= \sigma_{rr}\mathbf{e}_r\otimes\mathbf{e}_r+\sigma_{\theta\theta}\mathbf{e}_\theta\otimes\mathbf{e}_\theta+\sigma_{\theta z}(\mathbf{e}_\theta\otimes\mathbf{e}_z+\mathbf{e}_z\otimes\mathbf{e}_\theta)\\ &\quad+\sigma_{zz}\mathbf{e}_z\otimes\mathbf{e}_z,\end{aligned} \tag{22}$$

where

$$\sigma_{rr} = -p+\frac{\mu\nu R^2}{\lambda_z^2r^2}, \tag{23}$$

$$\begin{aligned}\sigma_{\theta\theta} &= -p+\frac{\mu r^2}{\nu}(\kappa^2+\frac{1}{R^2})\\ &\quad+\frac{2\gamma r^2}{\nu}(\kappa\cos\beta+\frac{1}{R}\sin\beta)^2(I_4-1),\end{aligned} \tag{24}$$

$$\sigma_{zz} = -p+\frac{\mu}{\nu}\lambda_z^2+\frac{2\gamma}{\nu}\lambda_z^2(I_4-1)\cos^2\beta, \tag{25}$$

$$\begin{aligned}\sigma_{\theta z} &= \frac{\mu}{\nu}\kappa\lambda_z r+\frac{2\gamma}{\nu}\lambda_z r\cos\beta(\kappa\cos\beta\\ &\quad+\frac{1}{R}\sin\beta)(I_4-1).\end{aligned} \tag{26}$$

This framework is built on strain energy functions and general deformation gradients, and it is thus valid for both small and large deformations.

B. Boundary Conditions

The boundary conditions on the conjugated polymer actuator are specified as follows:

$$\sigma_{rr}|_{R=R_i}=0,\ \ \sigma_{rr}|_{R=R_o}=0, \tag{27}$$

which represent that there is no direct loading applied to the inner and outer lateral surfaces. Note that R is used in (27) since r is also a function of R. The equilibrium equation $\mathrm{div}\sigma=0$ in the directions of r, z, and θ can be written as follows:

$$\frac{\partial\sigma_{rr}}{\partial r}+\frac{1}{r}\frac{\partial\sigma_{r\theta}}{\partial\theta}+\frac{\partial\sigma_{rz}}{\partial z}+\frac{1}{r}(\sigma_{rr}-\sigma_{\theta\theta})=0, \tag{28}$$

$$\frac{\partial\sigma_{rz}}{\partial r}+\frac{1}{r}\frac{\partial\sigma_{\theta z}}{\partial\theta}+\frac{\partial\sigma_{zz}}{\partial z}+\frac{\sigma_{rz}}{r}=0, \tag{29}$$

$$\frac{\partial\sigma_{r\theta}}{\partial r}+\frac{1}{r}\frac{\partial\sigma_{\theta\theta}}{\partial\theta}+\frac{\partial\sigma_{z\theta}}{\partial z}+\frac{2\sigma_{r\theta}}{r}=0, \tag{30}$$

where $\sigma_{r\theta}=0$, $\sigma_{rz}=0$ in this case. Considering (24), (25), and (26), one can show that (29) and (30) reduce to $\frac{\partial p}{\partial z}=0$ and $\frac{\partial p}{\partial\theta}=0$, which means that p is a function of r only. Given $\sigma_{r\theta}=0$ and $\sigma_{rz}=0$, one can write (28) as follows by using (8):

$$\frac{d\sigma_{rr}}{dR}=-\frac{\nu R}{\lambda_z r^2}(\sigma_{rr}-\sigma_{\theta\theta}), \tag{31}$$

which can be furthermore expanded by considering (23):

$$\frac{dp}{dR} = \frac{\nu R}{\lambda_z r^2}(\sigma_{rr} - \sigma_{\theta\theta}) + \frac{\mu\nu}{\lambda_z^2}\frac{d}{dR}(\frac{R^2}{r^2}). \quad (32)$$

Integrating (32) after substituting the expression of (23) minus (24), one can obtain an expression for p by using the boundary condition $\sigma_{rr}|_{R=R_0} = 0$:

$$p = \frac{\nu R^2\mu}{\lambda_z^2 r^2} - \int_R^{R_0}(\mu(\frac{\nu^2 R^3}{\lambda_z^3 r^4} - \frac{R(R^2\kappa^2+1)}{\lambda_z R^2}) - \frac{2R\gamma}{\lambda_z}(\kappa cos\beta + \frac{1}{R}sin\beta)^2(I_4 - 1))dR. \quad (33)$$

Applying the other boundary condition $\sigma_{rr}|_{R=R_i} = 0$ in (33) gives the following constraint equation:

$$\Delta = 0, \quad (34)$$

where

$$\Delta = \int_{R_i}^{R_o}(\frac{\mu}{2}(-\frac{\nu^2 R^2}{\lambda_z^2 r^4} + \kappa^2 + \frac{1}{R^2}) + (\kappa\cos\beta + \frac{1}{R}sin\beta)^2\gamma(I_4 - 1))RdR. \quad (35)$$

C. Nonlinear Model

One can see from Fig. 3 that three variables quantify the deformed configuration: r, λ_z, and κ. Because the profile of r can be calculated based on (9), the variable r can be replaced by r_i to characterize the deformation together with the other two variables. Eq. (35) has provided one constraint equation. The other two require knowledge of the moment T and axial load P, which are given by the following expressions:

$$T = 2\pi\int_{r_i}^{r_o}\sigma_{\theta z} r^2 dr, \quad (36)$$

$$P = 2\pi\int_{r_i}^{r_o}\sigma_{zz} r dr. \quad (37)$$

When one end of the tube is not constrained, it follows that $T = 0$ and $P = 0$. These two equations, along with (34), provide three nonlinear equations for r_i, κ, and λ_z. One finds that: the expression (35) is strongly dependent on r_i, the expression (36) for T is strongly dependent on κ, and the expression (37) for P is strongly dependent on λ_z. In general, the numerical analysis to obtain these variables by solving three nonlinear equations is difficult. Therefore, in this paper, λ_z, representing the length change ratio in the axial direction, will be measured and used as a given parameter. Since Δ and T give the strongest dependence on r_i and κ, the equations $\Delta = 0$ and $T = 0$ are retained in the analysis and numerically solved to obtain r_i and κ. By substituting from (26), one can integrate (36) and obtain the following expression:

$$T = \mu a\kappa + \gamma(b_0 + b_1\kappa + b_2\kappa^2 + b_3\kappa^3), \quad (38)$$

where a, b_0, b_1, b_2 and b_3 are terms involving material constants. Similarly one can integrate (35) and obtain the expression for Δ as follows:

$$\Delta = \mu\Omega + \gamma\Gamma, \quad (39)$$

where Ω and Γ are also terms involving material properties and λ_z, κ, and r_i, which will not be listed in this paper due to the page limitation. The two unknown variables r_i and κ can be obtained by numerically solving the coupled equations $\Delta = 0$ and $T = 0$ using (38) and (39).

IV. Experimental Results

A. Actuator Fabrication

To fabricate the actuator, it is crucial to integrate the fibers into the material matrix of PPy. This would ensure that, when the PPy tube volume changes, the torsional motion will be generated when the motion in other directions are constrained. For this purpose, firstly a glass cylinder with a diameter of 2.5 mm is used as the substrate and coated uniformly with gold through sputtering. Then a platinum wire with diameter of 25 μm is wound uniformly along the glass cylinder. The pitch angle β is 80^o. This tube is soaked in the electrolyte (0.05M LiTFSI in Propylene Carbonate) and connected to the working electrode of a potentiostat (OMNI101 from Cypress Systems). An electrochemical deposition process is conducted by following the method in [20]. To maintain a constant potential on PPy when PPy grows on the surface of glass tube, an Ag/AgCl reference electrode (Aldrich Chemical) is used. The auxiliary electrode is a stainless steel mesh. The electrolyte used in experiment is a mixed solution of 0.1M pyrrole, 0.1M LiTFSI in Propylene Carbonate with 0.5w/w% water. The current density is maintained at 2 mA/cm^2 for a total period of 20 hours. A PPy tube with wall thickness of 250 μm is grown on the tube surface, which integrates the platinum wire. Because the sputtered gold layer has poor adhesion force with the PPy inner surface, the PPy tube can be easily taken off from the glass cylinder. Fig. 5 shows the fabricated prototype. The inner diameter of the tube is 2.5 mm, and the outer diameter is 3 mm.

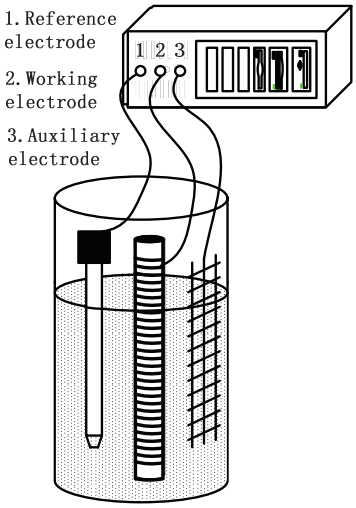

Fig. 4. The experimental setup to fabricate the fiber reinforced conjugated polymer actuator.

B. Experimental Setup for Characterizing the Actuator

The PPy tube is soaked in 0.1M LiTFSI in Propylene Carbonate (PC), with the top out of electrolyte for electric

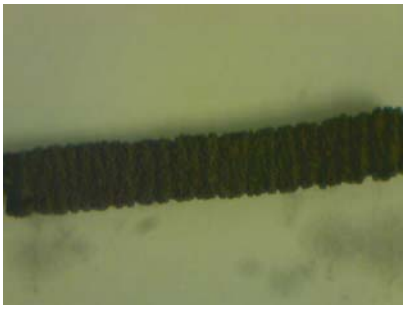

Fig. 5. Fabricated platinum fiber-reinforced PPy tube.

contact. A voltage is applied across the PPy tube and the counter electrode, which is a stainless steel mesh in the experiments. A computer equipped with a DS1104 R&D Controller Board (dSPACE Inc) is used for data acquisition and processing. A laser distance sensor (OADM 20I6441/S14F, Baumer Electric) with resolution of 4 μm is used to measure the motion of the actuator. Sticky copper film is attached to different positions of the PPy tube for measurement purposes. Three motion signals are measured, which are the inner radius r_i, torsional displacement y at the end of the tube as shown in Fig. 6, and the length change at the end of the tube that equals to $\lambda_z \cdot L$ based on (4), where L is the length of the PPy tube. The model predicted variables r_i and λ_z can be correlated directly to the measured variables, while κ is obtained based on the geometric relationship in Fig. 6:

$$y = R_m \tan(\kappa \cdot L), \tag{40}$$

where y is the measured displacement, L is 17.2 mm, and R_m is 5 mm in this paper.

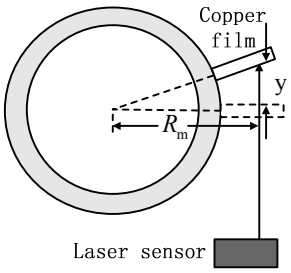

Fig. 6. Experimental setup to measure κ. The copper film is attached perpendicular to the outer surface at the tube bottom.

C. Experimental Results and Discussions

The quasi-static response is studied by applying a low frequency sinusoidal voltage on the actuator. The frequency is chosen to be 0.01 Hz to allow the actuator to reach the quasi-static condition. The peak magnitudes of the responses under AC voltages of different amplitudes are shown in Fig. 7. The sinusoidal voltage amplitude is varied from 2 V to 4 V. Note that since only one laser sensor is available, measurements of inner radius, torsional displacement, and length change are performed separately and then synchronized through the voltage signal. One interesting phenomenon observed in experiments is that the inner radius and torsional displacement signals have reversed phases. In particular, when the inner radius decreases, the torsional displacement increases. The Young's moduli of platinum and PPy are chosen to be 280 GPa and 80 MPa in model prediction [15], [21]. From Fig. 7, the model can predict both inner radius and torsional displacement well within the voltage range, and the reversed phase of these two signals. Note that there are no experimental data points for the inner radius when the input voltage is lower than 2.8 V, since the inner radius response is beyond the resolution of the laser sensor when the maximum voltage input is smaller than 2.8 V.

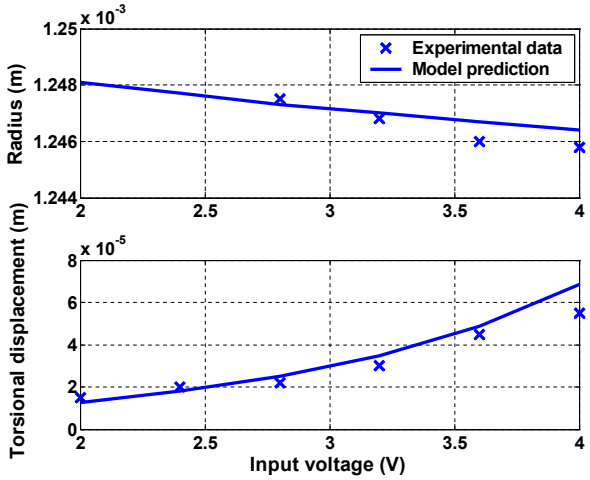

Fig. 7. Comparison of inner radius and torsional displacement between the model prediction and experiments. The input voltage represents the amplitude of the applied 0.01 Hz sinusoidal signal, and each data point is collected when the instantaneous value of the input reaches the peak.

The deformation signals under the AC voltage with amplitude 4 V are shown in the following figures: Fig. 9 for the inner radius, Fig. 10 for the torsional displacement, and Fig. 8 for the length change. As discussed in Sec. III-C, the length change is used to obtain λ_z and taken as a given parameter to reduce the difficulties in numerical analysis. Therefore the model predicted inner radius and torsional displacement are compared with the experimental data in Fig. 9 and Fig. 10. As one can see, the model can predict the experimental data well. It also predicts correctly the reversed phase in inner radius and torsional displacement.

V. Conclusions

Experiments have shown that the tube-shaped conjugated polymer actuator can generate torsional deformation when an actuation voltage is applied across the conjugated polymer and the electrolyte. A nonlinear elasticity-based model has been utilized to capture the actuator performance, which holds for both small and large deformations. The effectiveness of the model has been validated with experimental results.

Future work includes fabrication of the conjugated polymer tube with different configurations, such as different tube

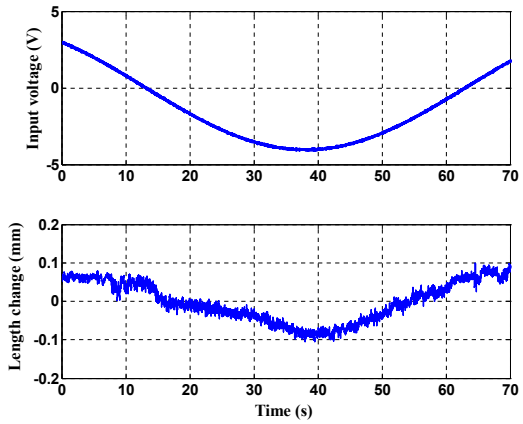

Fig. 8. The change of tube length with 0.01 Hz sinusoidal voltage input.

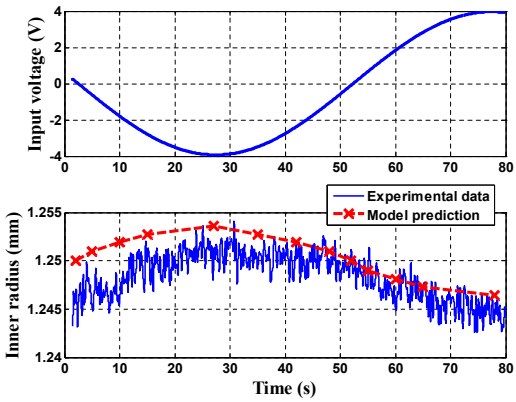

Fig. 9. The change of inner radius with 0.01 Hz sinusoidal voltage input.

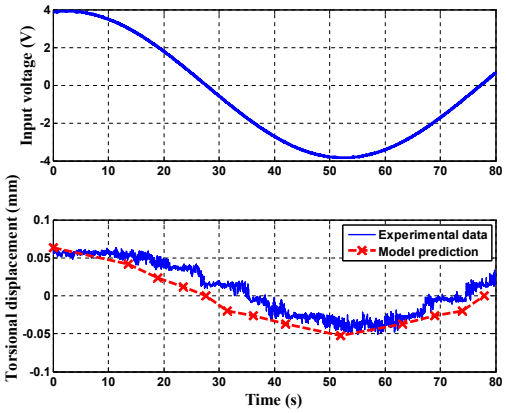

Fig. 10. The torsional displacement with 0.01 Hz sinusoidal voltage input.

thickness and wire winding angle β, utilizing the nonlinear elasticity model to predict the actuator performance, and optimizing the actuator designs for different applications.

VI. ACKNOWLEDGMENTS

The authors would like to thank Prof. Hasan Demirkoparan at Carnegie Mellon University in Qatar for helpful discussions regarding the nonlinear model.

REFERENCES

[1] R. Baughman, "Conducting polymer artificial muscles," *Synthetic Metals*, vol. 78, pp. 339–353, 1996.

[2] E. Smela, "Conjugated polymer actuators for biomedical applications," *Journal of Advanced Materials*, vol. 15, no. 6, pp. 481–494, 2003.

[3] G. G. Wallace, G. M. Spinks, L. Kane-Maguire, and P. R. Teasdale, *Conductive Electroactive Polymers: Intelligent Materials Systems (2nd Edition)*. Boca Raton, FL: CRC Press LLC, 2003.

[4] Y. Wu, D. Zhou, G. Spinks, P. Innis, and G. Wallace, "Titan: A conducting polymer based microfluidic pump," *Smart Marterials and Structures*, vol. 14, pp. 1511–1516, 2005.

[5] C. Immerstrand, K. H. Peterson, K.-E. Magnusson, E. W. H. Jager, M. Krogh, M. Skoglund, A. Selbing, and O. Inganas, "Conjugated-polymer micro- and milliactuators for biological applications," *Materials Research Society Bulletin*, vol. 27, no. 6, pp. 461–464, 2002.

[6] E. Smela, M. Kallenbach, and J. Holdenried, "Electrochemically driven polypyrrole bilayers for moving and positioning bulk micromachined silicon plates," *Microelectromechanical Systems*, vol. 8, no. 4, pp. 373–383, 1999.

[7] Y. Fang and X. Tan, "Design and modeling of a petal-shape, conjugated polymer-actuated micropump," in *Proceedings of the 1st ASME Dynamic Systems and Control Conference*, Ann Arbor, MI, 2008, paper DSCC2008-2278.

[8] Y. Fang, X. Tan, and G. Alici, "Robust adaptive control of conjugated polymer actuators," *IEEE Transactions on Control Systems Technology*, vol. 14, no. 6, pp. 600–612, 2008.

[9] T. J. Pence and H. Tsai, "Swelling induced cavitation of elastic spheres," *Mathematics and Mechanics of Solids*, vol. 11, pp. 527–551, 2006.

[10] J. Merodio and R. W. Ogden, "Mechanical response of fiber-reinforced incompressible non-linearly elastic solids," *International Journal of Non-Linear Mechanics*, vol. 40, pp. 213–227, 2005.

[11] Z. Guo, X. Peng, and B. Moran, "Mechanical response of neo-hookean fiber reinforced incompressible nonlinearly elastic solids," *International Journal of Solids and Structures*, vol. 44, pp. 1949–1969, 2006.

[12] H. Demirkoparan and T. J. Pence, "Torsional swelling of a hyperelastic tube with helically wound reinforcement," *Journal of Elasticity*, vol. 92, pp. 61–90, 2007.

[13] J. Ding, L. Liu, G. M. Spinks, D. Zhou, G. G. Wallace, and J. Gillespie, "High performance conducting polymer actuators utilising a tubular geometry and helical wire interconnects," *Synthetic Metals*, vol. 138, pp. 391–398, 2003.

[14] Y. Fang, X. Tan, and G. Alici, "Redox level-dependent impedance model for conjugated polymer actuators," *Sensors and Actuators B: Chemical*, vol. 132, pp. 182–190, 2008.

[15] Y. Fang, T. Pence, and X. Tan, "Nonlinear elastic modeling of differential expansion in trilayer conjugated polymer actuators," *Smart Materials and Structures*, vol. 17, pp. 65 020: 1–10, 2008.

[16] Q. Pei and O. Inganäs, "Electrochemlcal applIcatlons of the bending beam method. 1. mass transport and volume changes in polypyrrole during redox," *Journal of Physical Chemistry*, vol. 96, pp. 10 507–10 514, 1992.

[17] J. D. W. Madden, "Conducting polymer actuators," PhD thesis, MIT, 2000.

[18] S. Therkelsen, "Constitutive modeling of active polymers," Master thesis, MIT, 2005.

[19] G. Qiu and T. Pence, "Remarks on the behavior of simple directionally reinforced incompressible nonlinearly elastic solids," *Journal of Elasticity*, vol. 49, pp. 1–30, 1997.

[20] G. Alici, P. Metz, and G. M. Spinks, "A methodology towards geometry optimization of high performance polypyrrole (PPy) actuators," *Smart Materials and Structures*, vol. 15, pp. 243–252, 2006.

[21] K. Chen, L. Zhao, J. Tse, and J. Rodgers, "Elastic properties of platinum rh and rh3x compounds," *Physics Letter A*, vol. 331, pp. 400–403, 2004.